

Non-planar geometries of solution processable transparent conducting oxide: from film characterization to architected electrodes†

Moe Kevin, Gah Hung Lee and Ghim Wei Ho*

Received 6th February 2012, Accepted 20th March 2012

DOI: 10.1039/c2ee21296j

Transparent conducting Ga : ZnO films were synthesized directly on glass substrates *via* a low-temperature aqueous route for application in dye-sensitized solar cells. Preliminary electrical and optical characterization of the films showed that 85% transparency across the optical range with sheet resistances as low as $15 \Omega \text{ sq}^{-1}$ were achievable, making them comparable to commercial transparent conducting oxides. Novel non-planar transparent conducting electrodes consisting of pillars, cross-hatched trenches and pit structures were fabricated to produce films with increased surface roughness and enhanced light scattering capabilities which are essential for photovoltaic applications. The work concludes with proof of concepts demonstrating the feasibility of large-scale fabrication and the compatibility of the electrodes for dye-sensitized solar cells.

1. Introduction

Transparent conductors (TCs) play a critical role in solar cells and have seen a heightened prominence amongst consumers and researchers in recent years: the development of cost effective and energy efficient solar cells hinge on the availability of low cost and high performance TCs. One can easily appreciate the motivations behind the researchers' goal in recent years of finding new TCs materials that meet the electrical and optical requirements as well as keeping low fabrication cost in a bid to cater for the ever growing demand of consumers, energy consumption and conservation. The performance of solar cells is affected by TCs in two ways; transmission of optical incident light and transmission of electrical power through the TCs layer by transportation of optically generated carriers. As such, output power optimization

is possible with high optical transparency and low sheet resistance TCs.

Wide bandgap metal-oxide semiconductors, such as indium tin oxide, have been traditionally used as TCs for various types of solar cells. Metal oxides are still by far the most prevalent form of TC because of their low resistivities, excellent transparency, environmental stability and compatibility for solar cell applications. However, the high cost of indium has spurred the development of alternatives such as suitably doped zinc oxide and tin oxide based TCs. These TCs are commonly deposited using high cost vacuum deposition techniques such as sputtering, pulsed laser deposition (PLD) and chemical vapour deposition (CVD). Metal oxides aside, recent developments of TCs include the use of metallic nanowires meshes, conducting polymers, as well as carbon allotropes like carbon nanotubes (CNTs) and graphene.¹⁻⁵

The benefits of fabricating ZnO TCs and employing low temperature aqueous synthesis are many fold. Firstly, ZnO has high abundance compared to the other oxide TC materials. Another advantage of ZnO is its stability in a hydrogen

Department of Electrical and Computer Engineering, National University of Singapore, 4 Engineering Drive 3, 117576, Singapore. E-mail: elehgw@nus.edu.sg

† Electronic supplementary information (ESI) available. See DOI: 10.1039/c2ee21296j

Broader context

The transparent conductor industry is one of the fastest-growing markets because of ever increasing demands. Transparent conductors are cornerstone components in a variety of optoelectronic and energy harvesting devices. In recent years, there has been immense interest in the development of new transparent conducting materials that use cheap precursors, low temperature synthesis with the added benefits of scalability. Non-planar transparent conductors have also been developed as part of increasing efforts to boost the performances of photovoltaic devices through light scattering and increasing surface roughness. However, not much has been reported as they are not easily fabricated using the traditional vapour deposition processes. This work features the fabrication of non-planar transparent electrodes *via* an aqueous route, paving the way for new device architectures which will be of interest to the photovoltaic community.

atmosphere, e.g., silane (SiH_4) plasma discharge production of Si : H thin film solar cells. Production cost is greatly reduced because of the minimal investment of low thermal energy ($<100^\circ\text{C}$) required for such growth. Furthermore, the process does not require high-maintenance and expensive vacuum pumps and chambers which are associated with vapour deposition. Aqueous synthesis also offers unparalleled scalability. Numerous films are simultaneously grown, thus increasing the production rate. Lastly, the synthesis is based on green chemistry and does not pose any significant process hazard or environmental concern.

This work focuses on the fabrication of TCs for use in photovoltaic devices. Current trends in DSSC research has made extensive use of three-dimensional photoanodes by means of photonic crystals, mesoporous structures and metal oxide fibrous networks. Such structures were used to improve light harvesting and charge transport within the device.^{6,7} In this work, we report for the first time dye sensitized solar cells (DSSC) based on fully solution-processable fabrications of textured single crystal ZnO transparent electrodes on glass with a ZnO photoactive nanoparticle film. We have carried out a comprehensive structural, electrical and optical understanding needed for the development of a new transparent conductor for solar cells. By further exploiting the low-temperature nature of the growth process with lithography, we fabricated novel TC electrodes which are not restricted to planar-geometries to create interesting structures. The work then concludes with a comparison between DSSC devices fabricated using the Ga : ZnO films and commercial ITO. Power conversion efficiency attained by the Ga : ZnO electrode solar cell is compared to the conventional ITO electrode and demonstrations on 7.2 inch glass substrate are presented.

2. Experimental section

2.1. Colloidal ZnO nanoparticle synthesis

Colloidal ZnO nanoparticles were synthesized by adding methanolic solutions of potassium hydroxide (15 mL, 0.41 mM) to zinc acetate dihydrate (30 mL, 0.11 mM) in a drop-wise fashion. The zinc acetate solution was then capped and was kept under constant stirring at 60°C using a water bath. After 90 min, the ZnO colloids were washed by centrifuging 3 times in methanol and finally dispersed in 10 mL of methanol and 5 mL of chloroform. The colloidal solution was stable for several months.

2.2. Ga : ZnO film growth

1.0 cm \times 1.0 cm borosilicate glass (Schott) were first cleaned in DI water, acetone and isopropyl alcohol (IPA) for 3 min each using an ultrasonic bath. The substrates were then dip-coated in a colloidal solution of ZnO nanoparticles. The growth solution was prepared by adding aqueous ammonia (33%) to 50 mM of aqueous zinc nitrate hexahydrate in order to adjust its pH to 10.85. Trisodium citrate and a gallium nitrate nonahydrate were added as surfactant and dopant, respectively. The pre-seeded glass substrates were immersed vertically in a reaction vessel containing the growth solution and allowed to stand in a convection oven for 4 hours at 90°C . Following the growth, the substrates were removed and sonicated in ethanol for 1 min to remove any surface particles and finally dried in a stream of N_2 gas.

2.3. Film characterization

SEM characterization was carried out using a JEOL FEG JSM 6700F field-emission scanning electron microscope operating at 15 kV with a built-in energy dispersive X-ray (EDX) attachment (Oxford Instrument and Inca software). TEM images were obtained using a JEOL-2100 high-resolution transmission electron microscope with an accelerating voltage of 200 kV. X-ray diffraction was carried out on a Philips X-ray diffractometer with Cu $K\alpha$ radiation ($\lambda = 1.541 \text{ \AA}$). Transmission spectra were obtained using a Shimadzu UV-3600 UV-vis spectrophotometer with integrating sphere assembly. The Hall measurement was performed at room temperature by a Bio-Rad Hall system on 1 cm by 1 cm sample using the Van der Pauw configuration. Indium was used to create an ohmic contact with the Ga : ZnO film.

2.4. Solar cell fabrication and testing

Dye sensitized solar cells were fabricated using Ga : ZnO as the anode and counter electrode. Commercial ZnO nanoparticles (Aldrich) were 'doctor bladed' onto the TC as a photoanode, and subsequently annealed at 350°C for 30 min in a muffled furnace. The photoanode was then soaked in an ethanolic solution of N719 dye for 1 hour. For Pt counter electrodes, 15 nm of Pt was sputtered using DC magnetron sputtering. For carbon electrodes, a 2B pencil was used to 'colour' the TC. The redox electrolyte was prepared with 0.1 M LiI, 0.05 M I_2 , 0.6 M 1,2-dimethyl-3-propylimidazolium iodide, and 0.5 M 4-*tert*-butylpyridine in acetonitrile. All devices were tested under AM1.5 conditions using a Newport 91160A solar simulator. The light source comprised a 150 W Xe lamp and the light intensity corresponded to AM1.5 (100 mW cm^{-2}) calibrated with a standard Si cell (Oriel SRC1000 TC).

3. Results and discussions

3.1. Growth and material characterization

Systematic studies on aqueous ammonia systems containing zinc nitrate have shown that zinc ions undergo retrograde solubility.⁸

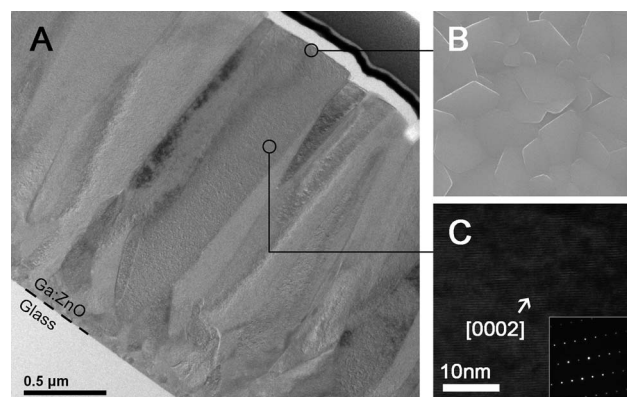


Fig. 1 (A) Cross-section TEM images of ZnO films grown on glass showing the grain structure. (B) Top-view SEM image of ZnO film. (C) HR-TEM image of a single-crystal grain within the film. Inset: SAED pattern.

When the system becomes supersaturated at 70–90 °C, ZnO homogeneously nucleates favourably onto substrates pre-seeded with ZnO, or heterogeneously onto nearly lattice matching substrates. Few groups have successfully reported ZnO films growth *via* low temperature aqueous synthesis or similar techniques on epitaxial substrate: Le *et al.*⁹ and Andeen *et al.*¹⁰ previously reported the growth of ZnO thin film on an epitaxial MgAl₂O₄ (111) substrate by hydrothermal means. Kim *et al.*¹¹ have also reported the hydrothermal growth of ZnO thin film on epitaxial GaN buffered sapphire. These reports of hydrothermal ZnO thin films are based on heteroepitaxial film growth, *i.e.* ZnO deposited on costly nearly lattice matched substrates.

Subsequently, our work is focused on single-crystalline textured films on glass. ZnO crystals were grown on glass which were pre-seeded with colloidal ZnO nanoparticles, in the form of nanowires. To obtain smooth ZnO films, trisodium citrate (Na₃C₆H₅O₇) was added to the growth solution to act as a surfactant. The effect of citrate ions was to promote lateral

growth of the nanowires, eventually causing them to coalesce into a continuum. The negatively charged citrate ions adhered to the positively charged Zn-terminated (0001) plane, thus retarding the growth in the [0002] direction (*c*-direction) while growth rate in the lateral [10 $\bar{1}$ 0] direction remains unchanged.¹²

Fig. 1A shows the transmission electron microscope (TEM) cross section of said film on a glass substrate. The film was found to comprise large single-crystal grains which emanated from the glass interface. Fig. 1B is a scanning electron microscope (SEM) image of the film surface showing hexagonal shaped grains which are characteristic of the ZnO *c*-plane. The SEM image also indicated that the surface was smooth and devoid of discontinuities. This was essential for good transparency because surface irregularities serve to scatter light. Fig. 1C shows the high resolution TEM (HR-TEM) image of a single-crystal grain with the corresponding selected area electron diffraction (SAED) pattern. The grains were highly *c*-oriented in the out-of-plane direction, and had an average diameter of 500 nm (measured at the surface). However, these diameters were generally found to increase with film thickness. This led to the Ga : ZnO films to possess grains which were at least 10 times larger than films deposited by sol-gel or vacuum based techniques.

In order to dope the films with Ga ions, gallium nitrate (Ga(NO₃)₃) was added to the growth system. Energy dispersive X-ray spectroscopy (EDX) was used to provide a semi-quantitative determination of elemental concentrations up to depths of a few microns below the surface. Fig. 2A shows the EDX spectra of doped and undoped films. Prominent peaks of Zn K α ₁ at 8.638 keV and K β ₁ at 9.572 keV, and the relatively weaker Ga peak at 9.251 keV ascribed to the K α ₁ transition were clearly observed. The atomic percentage of Ga was found to

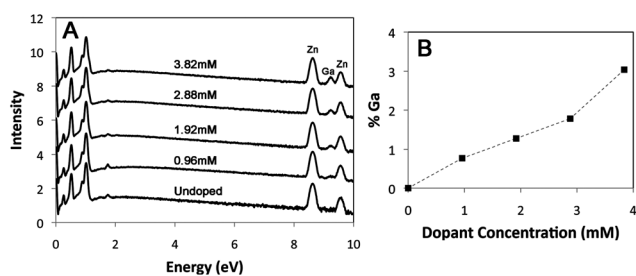


Fig. 2 (A) EDX spectra of Ga : ZnO films grown with different dopant concentrations. (B) Atomic percentages of Ga within the films.

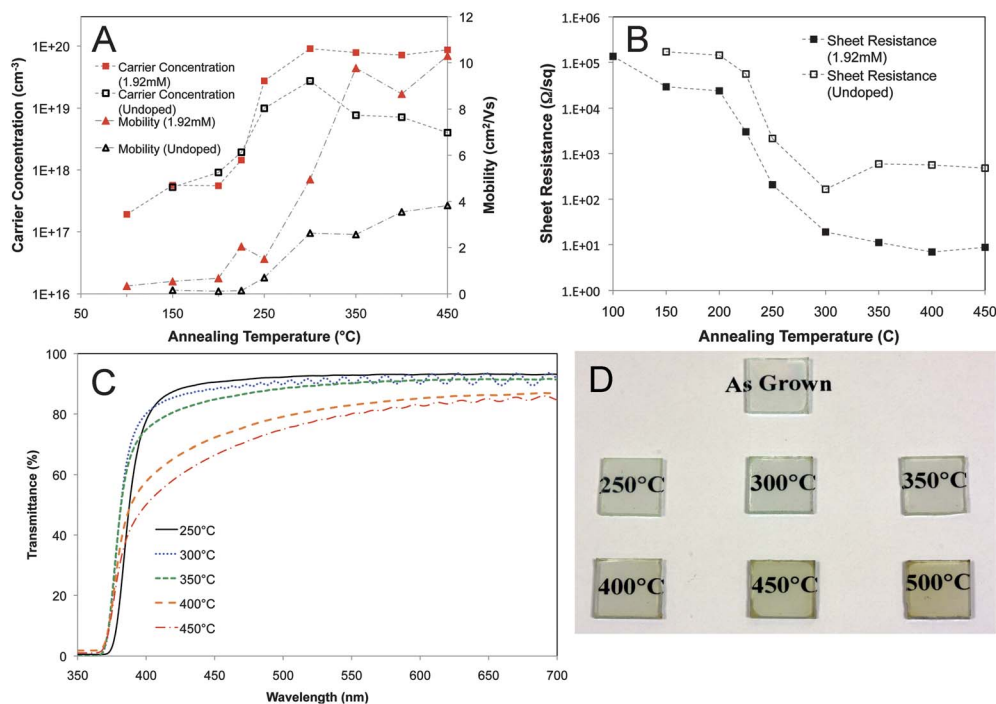


Fig. 3 (A) Carrier concentrations and mobilities of undoped and 1.92 mM doped films annealed between 150 °C and 450 °C. (B) Corresponding sheet resistances of undoped and 1.92 mM doped films. (C) Transmittance spectra of 1.92 mM doped films grown on 1 cm × 1 cm glass substrates annealed between 250 °C and 500 °C. (D) Digital image of films annealed at different temperatures.

approximately increase linearly with the dopant concentration (Fig. 2B), indicating that the presence of Ga was a direct consequence of the $\text{Ga}(\text{NO}_3)_3$ added.

3.2. Electrical and optical properties

As aqueous synthesis occurs at low temperatures, post annealing was required to activate the dopant species. In order to study effects of the post annealing temperatures, undoped and 1.92 mM doped films were annealed at various temperatures ranging from 100 °C to 450 °C. The carrier concentrations and mobilities are plotted in Fig. 3A. The graph shows that the mobility and carrier concentration increased abruptly at different temperature ranges. For carrier concentration, the increase is observed between 225 °C and 300 °C. At 300 °C, the maximum carrier concentration of $9.1 \times 10^{19} \text{ cm}^{-3}$ was attained for doped films. Further increase of annealing temperature (>300 °C) showed no change in carrier concentration for the doped films, while the undoped films displayed a consistent drop to $4.0 \times 10^{18} \text{ cm}^{-3}$.

With regards to the changes in mobility with temperature, it is observed that films annealed below 250 °C had an average mobility of $0.8 \text{ cm}^2 \text{ Vs}^{-1}$. A sudden increase in mobility was observed between 250 °C and 350 °C for both films, *i.e.* from $1.5 \text{ cm}^2 \text{ Vs}^{-1}$ to $9.8 \text{ cm}^2 \text{ Vs}^{-1}$ for doped samples, and $0.7 \text{ cm}^2 \text{ Vs}^{-1}$ to $4.9 \text{ cm}^2 \text{ Vs}^{-1}$ for undoped samples. The sheet resistances obtained are plotted in Fig. 3B, from which we note that values of $15 \Omega \text{ sq}^{-1}$ can be obtained at annealing temperatures as low as 350 °C. The best sheet resistance was $6.9 \Omega \text{ sq}^{-1}$ with a corresponding resistivity of $7 \times 10^{-3} \Omega \text{ cm}$.

The temperature dependence of carrier concentration can be understood by considering both the presence of Ga and role of hydrogen (H) species in the film. Density functional theory

calculations have revealed that H behaves exclusively as a donor in ZnO; it has been speculated to be primarily responsible for n-type behavior of ZnO films.¹³ n-type intrinsic defects such as oxygen vacancies and zinc interstitials produced deep donors and had large formation energies, respectively, making them improbable causes of n-type conductivity.^{14,15} Furthermore, H incorporation in low-temperature aqueous synthesis is especially high within the range of pH values used in this work because of the incomplete hydrolysis of zinc hydroxide complexes which results in the incorporation of hydrogen–oxygen complexes.^{16,17} Therefore, the initial rise in concentration between 200 °C and 225 °C was due to activation of H donors. This is further supported by the fact that both doped and undoped films exhibited the same increase, ruling out the possibility of Ga activation within this temperature range. We posit that Ga activation occurred primarily between 250 °C and 300 °C as the differences in concentration between doped and undoped films became apparent. At 350 °C and above, H started to get liberated from the film in the form of water vapor, in agreement with findings in the literature.¹⁸ This caused the marked decrease in carrier concentration in undoped films, whereas doped films showed no observable change in concentration because of the presence of Ga dopants.

With regards to mobility, the authors postulate that the increase of mobilities was due to the elimination of charged point defects after annealing. These are responsible for scattering carriers *via* electrostatic interaction. XRD measurements on films annealed at various temperatures did not indicate any noticeable change in the structural characteristics, suggesting that crystallinity does not play a major role in the increase of mobilities. Next, the generally low mobilities observed even at 450 °C ($10.2 \text{ cm}^2 \text{ Vs}^{-1}$) suggested that the main scattering mechanism was due to grain boundary scattering: Our work has

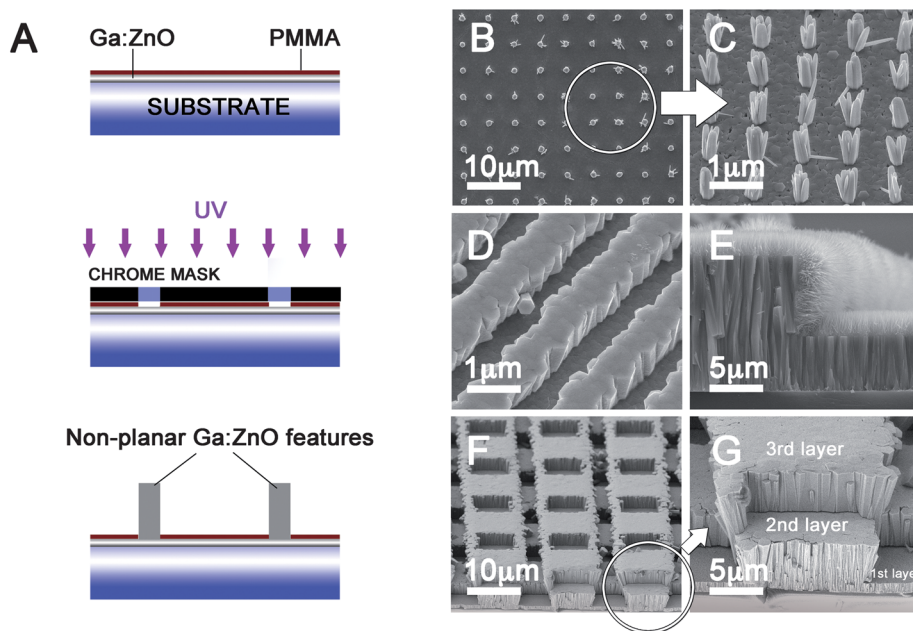


Fig. 4 (A) Schematic diagram describing the fabrication of non-planar-TC *via* the aqueous approach. (B) Top view of Ga : ZnO pillars grown from Ga : ZnO films. (C) 30 degree tilt of Ga : ZnO pillars with underlying film clearly visible. (D) 800 nm width Ga : ZnO trenches. (E) Conformally grown ZnO nanowires on a trench sidewall. (F) Multi-layer trenches and pits in a checker-board configuration. (G) Close up view of the multi-layer trenches.

shown that the same Ga : ZnO films grown on MgAl₂O₄ (111) exhibited a mobility of 31.8 cm² Vs⁻¹ with a carrier concentration of 1.1×10^{20} cm⁻³. These heteroepitaxial films grown on MgAl₂O₄ (111) had significantly fewer grain boundaries. Hence, grain boundary scattering is the dominant scattering mechanism for films on glass.

Fig. 3C shows the transmission spectra of the Ga : ZnO films post-annealed at various temperatures. The films exhibited transparencies of ~92% when annealed at 250 °C and ~88% at 300–350 °C at $\lambda = 500$ nm. Transparency started to degrade at 400 °C and above. These films darkened and exhibited a dull-orange tinge that persisted even after cooling down to room temperature. Transmission spectra indicated the films were initially less transparent to shorter wavelengths, while at 450 °C, the film transparency was degraded across the entire visible range. This was likewise observed on undoped ZnO films, and films grown on MgAl₂O₄ (111) and *c*-Al₂O₃, making this observation independent of influences from the dopant and substrate. Fig. 3D shows digital images of Ga : ZnO films on glass annealed at various temperatures clearly showing the gradual loss of transparency with increasing annealing temperatures.

3.3. Non-planar geometries and proof of concepts

The understanding gained from the post-annealing study demonstrated that post-annealing conditions could be used to vary sheet resistances. Such flexibility allows for a cost-effective means to optimize the TC properties to suit the desired application. For example, display and touch screen applications require high transparency (>90%) but only modest sheet resistance values (~100 to 1000 Ω sq⁻¹). Hence, Ga : ZnO annealed at 250 °C will suffice. For photovoltaic devices where low sheet resistances are essential, films annealed at 350 °C can give 10–20 Ω sq⁻¹ with an optical transparency greater than 85%.

Thus far, the results showed that Ga : ZnO films synthesized *via* an aqueous route constitutes a competitive alternative to existing commercial TCs. However, the advantage of aqueous synthesis over other techniques is made apparent when applied to the fabrication of TCs with non-planar geometries. In this work, we feature non-planar TC electrodes with periodic structures such as pillars and trenches that extend from an underlying Ga : ZnO film. Furthermore, the ease with which these TCs could be fabricated clearly distinguished the aqueous approach from other solution based sol–gel processes and vapour deposition techniques.

A schematic outlining this concept is shown in Fig. 4A. First, a Ga : ZnO film is grown on the substrate. Standard photolithographic steps were then used to pattern the Ga : ZnO film in order to selectively demarcate nucleation sites for a second stage of growth using aqueous synthesis again. In this work, PMMA was used as a photoresist together with an in-house DUV contact-lithography exposure system. Patterned Ga : ZnO films were immersed in the growth medium to create the structures. Since the initial Ga : ZnO film was *c*-oriented, the subsequent structures grew with similar orientation, resulting in *c*-aligned multi-layered patterned films. After growth, the photoresist was removed by sonicating the substrate in acetone. The structures constructed in Fig. 4B–G serve as examples of what can be

achieved using aqueous synthesis in conjunction with photolithography.

Fig. 4B and C show an array of Ga : ZnO pillars grown from a Ga : ZnO film. Such an aligned pillar array will prove useful in studying the charge transport properties of morphological composite dye-sensitized solar cells (DSSC) that integrate high surface area nanoparticles with aligned single-crystal Ga : ZnO pillars.^{19–23} This strategy permits precise control over the pillar pitch, diameter, height and placement which is critical for better integration of said morphologies.²⁴ Moreover, the integration of films and nanowires belonging to the same material system and

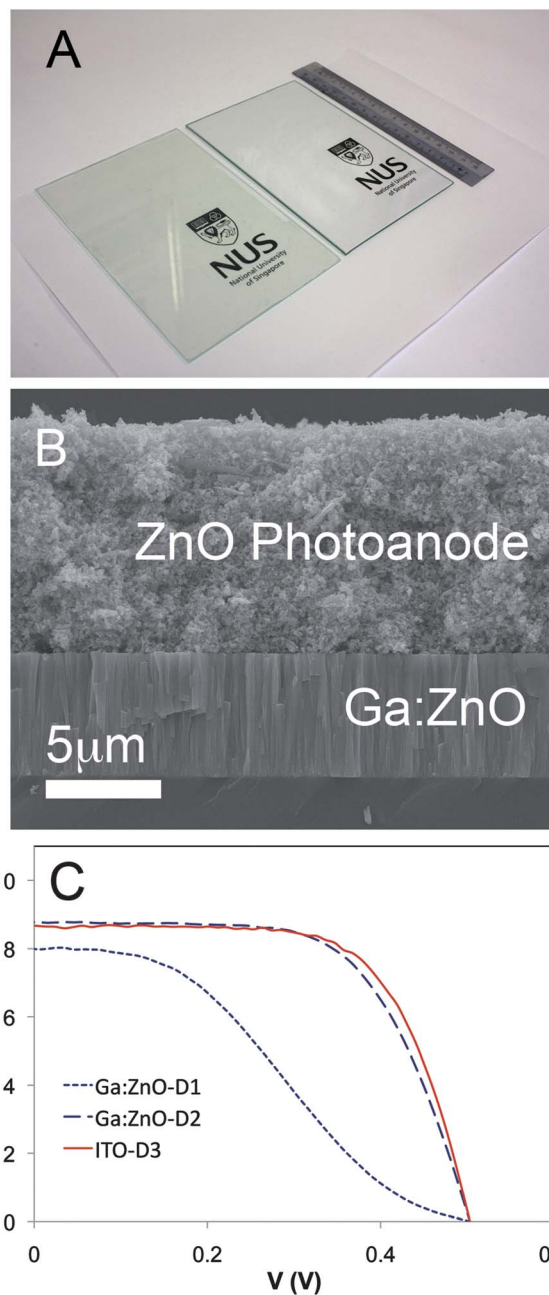


Fig. 5 (A) Large area growth of Ga : ZnO films on a glass panel. (B) ZnO nanoparticles doctor bladed onto Ga : ZnO film for DSSC. (C) J – V curves for DSSC.

Table 1 Summary of device parameters

Device	Anode	Counter electrode	Sheet resistance/ $\Omega \text{ sq}^{-1}$	η (%)	FF (%)	$J_{sc}/\text{A cm}^{-2}$	V_{oc}/V	R_s^a/Ω	R_{sh}^b (k Ω)
D1	Ga : ZnO	Ga : ZnO (Carbon)	20	1.39	34.3	7.98	0.51	920	5.03
D2	Ga : ZnO	Ga : ZnO (Pt)	20	2.82	62.9	8.78	0.51	76.6	18.6
D3	ITO	ITO (Pt)	15	2.89	66.3	8.67	0.50	58.5	35.7

^a R_s : series resistance. ^b R_{sh} : shunt resistance.

growth procedure guarantees barrier-less transport at the interface of the morphologies.

Fig. 4D shows Ga : ZnO strips grown on Ga : ZnO film. These trench features had near-vertical sidewalls which were a result of the *c*-oriented underlying film. The trenches simultaneously served as a light scattering layer as in a diffraction grating (see ESI[†]), while providing additional surface roughness for photoactive components.^{19,25} For example, ZnO nanowires were conformally grown over the trenches as shown in Fig. 4E. Fig. 4F and G show multi-layer Ga : ZnO trenches and pits grown in a cross hatch layout using 2 stages of lithography and 3 stages of growth.

It should be noted that the characteristic low temperatures used during the synthesis process were crucial factors in allowing for these interesting TCs. Further implementation and investigation of these novel TCs in photovoltaic devices will be comprehensively explored as part of our future work.

Lastly, we conclude this work with two proof of concepts. Firstly, large scale synthesis of Ga : ZnO films was performed on 7.2 inch glass panels. Fig. 5A shows the resulting substrate alongside a blank substrate for comparison. The film was likewise optically smooth and conductive, thus demonstrating that scaling up is feasible even in a laboratory setting. Next, a conventional ZnO nanoparticle based DSSC was fabricated using Ga : ZnO electrodes for both the photo and counter electrodes. Fig. 5B shows the cross section SEM image of a ZnO nanoparticle photoanode of 8 μm thickness ‘doctor bladed’ onto the Ga : ZnO film. The J - V curves of three different DSSCs (labeled D1-3) are plotted in Fig. 5C, and the corresponding device parameters are tabulated in Table 1. D1 and D2 used Ga : ZnO TCs for both the anode and counter electrodes. D1 consisted of Ga : ZnO ($20 \Omega \text{ sq}^{-1}$) with a carbon-coated counter electrode and had an efficiency, η , of 1.39%. Graphite coated by lead rubbing counter electrodes are known to give lower efficiencies than Pt counter electrodes because of its relatively poorer catalytic properties.^{26–28} Nevertheless, this showed that it is possible to fabricate DSSCs without employing any vacuum deposition process. Subsequently, devices D2 and D3 used Pt sputter coated counter electrodes. D2 comprised of Ga : ZnO films of $20 \Omega \text{ sq}^{-1}$, while D3 was fabricated using commercial ITO substrates of $15 \Omega \text{ sq}^{-1}$ as stated by the manufacturer. An efficiency of 2.82% and 2.89% was obtained for the Ga : ZnO and ITO electrodes, respectively, indicating that there was little difference in performance between the two. Other device parameters, such as the short circuit current density (J_{sc}), open circuit voltage (V_{oc}) and fill factors (FF) were likewise comparable since both devices were fabricated using the same ZnO photoanode structure, sensitizer and electrolyte. This is a strong indication that Ga : ZnO TCs grown *via* low-temperature

aqueous chemistry can function as a promising alternative for cost effective indium free and transparent conductors.

4. Conclusions

In summary, this work has demonstrated high performance solution processable textured Ga : ZnO films on glass for dye photovoltaic applications. This scalable procedure could be carried out without the need of sophisticated deposition chambers and occurs at a modest temperature of 90 °C. Fabrication of novel non-planar TCs was demonstrated to create electrodes with augmented surface roughness and improved light-scattering properties. Given the solution scalability and processability of high performance Ga : ZnO films, we anticipate the feasibility of large-scale TC production of alternatives of indium electrodes.

Acknowledgements

The authors would like to thank Connor Peh for his valuable input towards the fabrication of the dye sensitized solar cells, and the National University of Singapore for grant support (R-263-000-653-731).

Notes and references

- X. Wang, L. Zhi and K. Müllen, *Nano Lett.*, 2008, **8**, 323.
- K.-Y. Chun, Y. Oh, J. Rho, J.-H. Ahn, Y.-J. Kim, H. R. Choi and S. Baik, *Nat. Nanotechnol.*, 2010, **5**, 853.
- D. Zhang, K. Ryu, X. Liu, E. Polikarpov, J. Ly, M. E. Tompson and C. Zhou, *Nano Lett.*, 2006, **6**, 1880.
- H. Wu, L. Hu, M. W. Rowell, D. Kong, J. J. Cha, J. R. McDonough, J. Zhu, Y. Yang, M. D. McGehee and Y. Cui, *Nano Lett.*, 2010, **10**, 4242.
- J.-Y. Lee, S. T. Connor, Y. Cui and P. Peumans, *Nano Lett.*, 2008, **8**, 689.
- N. Tétrault and M. Grätzel, *Energy Environ. Sci.*, 2012, DOI: 10.1039/c2ee03242b.
- K. A. Arpin, M. D. Losego and P. V. Braun, *Chem. Mater.*, 2011, **23**, 4783.
- J. J. Richardson and F. F. Lange, *Cryst. Growth Des.*, 2009, **9**, 2570.
- H. Q. Le, S. K. Lim, G. K. L. Goh, S. J. Chua and J. Ong, *J. Electrochem. Soc.*, 2010, **157**, 796.
- D. Andeen, L. Loeffler, N. Padture and F. F. Lange, *J. Cryst. Growth*, 2003, **259**, 103.
- J. H. Kim, E.-M. Kim, D. Andeen, D. Thomson, S. P. DenBaars and F. F. Lange, *Adv. Funct. Mater.*, 2007, **17**, 463.
- S. Cho, J.-W. Jang, S.-H. Jung, B. R. Lee, E. Oh and K.-H. Lee, *Langmuir*, 2009, **25**, 3825.
- C. G. V. D. Walle, *Phys. Rev. Lett.*, 2000, **85**, 1012.
- A. Janotti and C. G. V. D. Walle, *Phys. Rev. B: Condens. Matter Mater. Phys.*, 2007, **76**, 165202.
- A. Janotti and C. G. V. D. Walle, *Appl. Phys. Lett.*, 2005, **87**, 122102.
- C. B. Tay, S. J. Chua and K. P. Loh, *J. Phys. Chem. C*, 2010, **114**, 9981.
- E. V. Lavrov, F. Börrnert and J. Weber, *Phys. Rev. B: Condens. Matter Mater. Phys.*, 2005, **71**, 035205.

- 18 K. Ip, M. E. Overberg, Y. W. Heo, D. P. Norton, S. J. Pearton, S. O. Kucheyev, C. Jagadish, J. S. Williams, R. G. Wilson and J. M. Zavada, *Appl. Phys. Lett.*, 2002, **81**, 3996.
- 19 P. Kuang, J.-M. Park, W. Leung, R. C. Mahadevapuram, K. S. Nalwa, T.-G. Kim, S. Chaudhary, K.-M. Ho and K. Constant, *Adv. Mater.*, 2011, **23**, 2469.
- 20 M. Law, L. E. Greene, J. C. Johnson, R. Saykally and P. Yang, *Nat. Mater.*, 2005, **4**, 455.
- 21 S. Yodyingyong, Q. Zhang, K. Park, C. S. Dandeneau, X. Zhou, D. Triampo and G. Cao, *Appl. Phys. Lett.*, 2010, **96**, 073115.
- 22 J. H. Noh, H. S. Han, S. Lee, J. Y. Kim, K. S. Hong, G.-S. Han, H. Shin and H. S. Jung, *Adv. Energy Mater.*, 2011, **1**, 829.
- 23 C.-H. Ku and J.-J. Wu, *Appl. Phys. Lett.*, 2007, **91**, 093117.
- 24 M. Kevin, Y. H. Fou, A. S. W. Wong and G. W. Ho, *Nanotechnology*, 2010, **21**, 315602.
- 25 S. H. Ko, D. Lee, H. W. Kang, K. H. Nam, J. Y. Yeo, S. J. Hong, C. P. Grigoropoulos and H. J. Sung, *Nano Lett.*, 2011, **11**, 666.
- 26 A. Kay and M. Gratzel, *Sol. Energy Mater. Sol. Cells*, 1996, **44**, 99.
- 27 W. J. Lee, E. Ramasamy, D. Y. Lee and J. S. Song, *Sol. Energy Mater. Sol. Cells*, 2008, **92**, 814.
- 28 K. Imoto, K. Takahashi, T. Yamaguchi, T. Komura, J. Nakamura and K. Murata, *Sol. Energy Mater. Sol. Cells*, 2003, **79**, 459.